

# Thermal and Structural Study of the Crystal Phases and Mesophases in the Lithium and Thallium(I) Propanoates and Pentanoates Binary Systems: Formation of Mixed Salts and Stabilization of the Ionic Liquid Crystal Phase

F. J. Martínez Casado,<sup>†</sup> M. Ramos Riesco,<sup>§</sup> I. da Silva,<sup>‡</sup> A. Labrador,<sup>†</sup> M. I. Redondo,<sup>§</sup> M. V. García Pérez,<sup>§</sup> S. López-Andrés,<sup>||</sup> and J. A. Rodríguez Cheda<sup>\*,§</sup>

BM16-Laboratori de Llum Sincrotó (LLS), c/o European Synchrotron Radiation Facility, 38043 Grenoble, France; BM25-Spline, c/o European Synchrotron Radiation Facility, 38043 Grenoble, France; Departamento de Química Física I, Facultad de Ciencias Químicas, Universidad Complutense, 28040 Madrid, Spain; and Departamento de Crystalografía y Mineralogía, Facultad de Ciencias Geológicas, Universidad Complutense, 28040 Madrid, Spain

Received: April 8, 2010; Revised Manuscript Received: June 18, 2010

The temperature and enthalpy vs composition phase diagrams of the binary systems  $[xC_2H_5CO_2Li + (1 - x)C_2H_5CO_2Tl]$ , and  $[x(n-C_4H_9CO_2Li) + (1 - x)n-C_4H_9CO_2Tl]$ , where  $x$  is the mole fraction, were determined by DSC. Both binary systems display the formation of one 2:1 mixed salt each (at  $x = 0.667$ ) that appear as a peritectic (incongruent melting) at  $T_{fus} = 512.0$  K, and  $T_{fus} = 461.1$  K, with  $\Delta_{fus}H_m = 13.76$  and  $8.08$  kJ·mol<sup>-1</sup> for Li–Tl (I) propanoates, and  $n$ -pentanoate mixed salts, respectively. The thermotropic liquid crystal of the thallium(I)  $n$ -pentanoate transforms into a more stable liquid-crystal phase, which appears in the phase diagram between 380 and 488 K and for  $x = 0$  up to  $x = 0.56$ . The crystal structure of thallium(I) propanoate and of the two mixed salts were obtained via X-ray synchrotron radiation diffraction measurements. These compounds present a bilayered structure similar to the two pure lithium salts previously found by our group.

## 1. Introduction

Polymorphism and/or polyomesomorphism are one of the most interesting aspects of the organic salts in general, and of metal alkanooates in particular. The stepwise melting process from the totally ordered crystalline phase at very low temperature until the isotropic liquid can be rather complicated, involving all of the transitions taking place as solid-to-solid, solid–mesophase, mesophase–mesophase, and melting. Thereby, different solid (plastic crystal, rotator,<sup>1,2</sup> or condit<sup>3</sup>) or fluid mesophases (liquid crystal), as well as polymorphs in the crystal phase can be found in these salts.

Although liquid-crystal formation in alkali soaps was discovered by Vorlander<sup>4</sup> in 1910, it is only after five decades that the organic salts are being widely studied, providing an important advance in the characterization of different mesophases. Many workers have studied in detail the mesomorphism of alkali, alkaline earth, and transition metal soaps, often finding very complex phase behavior. Numerous reviews<sup>5–14</sup> on organic salts and their formation of ionic liquid crystals are available.

The long-chain members of the organic salt series have received more attention than the short-chain ones because they form thermotropic mesomorphs more easily. The first member exhibiting thermotropic mesophase depends on the metal; e.g., for the sodium or thallium series, they are the propanoate and pentanoate members, respectively.<sup>5</sup> Mirnaya and co-workers<sup>15</sup> have investigated many binary phase diagrams of short-chain metal alkanooates and reported the surprising formation of

mesomorphism, even when none of both components are mesogens, but “potentially mesogenic compounds”. According to these authors, the reason for the appearance of an ionic liquid crystal mesophase would be the different size of the cations, which increases the electrical anisotropy of the carboxylates, favoring the formation of the liquid-crystal mesophases.

A variety of binary systems with common cations or common anions formed by alkali alkanooates have been analyzed, and some of them were reviewed and critically evaluated.<sup>16</sup> In particular, some of the already studied binary systems are the ones between lithium and cesium alkanooates, from formates to butyrates.<sup>17</sup> In these four cases, a mixed salt with the composition 2:1 between LiC<sub>*n*</sub>:CsC<sub>*n*</sub> (where  $n$  is the total number of carbons in the alkanooate anion, hereafter) is formed, and a liquid-crystal phase appears from the acetates mixture, even when the shortest members of the CsC<sub>*n*</sub> and LiC<sub>*n*</sub> series presenting mesogenicity are the ones with 6 and 12 C atoms, respectively. In addition, the formation of two mixed salts (with a composition of 1:1 and 2:1) and a stable liquid crystal phase was detected in the LiC<sub>4</sub>–RbC<sub>4</sub> binary system, studied by us.<sup>18</sup> The size of thallium(I) is comparable to the cesium or rubidium ones: thus, this cation could be appropriate in order to stabilize the probable liquid-crystal phase in the mixtures with LiC<sub>*n*</sub> compounds. Moreover, thallium(I) is a low polarizing cation that forms weaker bonds than alkali cations, and the melting points of TIC<sub>*n*</sub> compounds are much lower than those of the corresponding alkali carboxylates, and so the mesogenic phase in their binary systems are expected to appear at even lower temperatures than for pure TIC<sub>*n*</sub> members.

Thallium(I) and lithium alkanooates (TIC<sub>*n*</sub> and LiC<sub>*n*</sub>) have been widely studied in the past decades by several techniques, such as adiabatic calorimetry,<sup>19–30</sup> DSC,<sup>31–44</sup> DTA,<sup>45,46</sup> XRD,<sup>47,48</sup> and others.<sup>49</sup> However, many aspects about the thermal behavior,

\* Corresponding author. Tel.: +91-3944306. Fax: +91-3944135. E-mail: cheda@quim.ucm.es.

<sup>†</sup> BM16-Laboratori de Llum Sincrotó (LLS).

<sup>‡</sup> BM25-Spline.

<sup>§</sup> Departamento de Química Física I, Universidad Complutense.

<sup>||</sup> Departamento de Crystalografía y Mineralogía, Universidad Complutense.

**TABLE 1: Experimental Parameters and Main Crystallographic Data for the Studied Compounds**

data	TiC3	Li <sub>2</sub> Tl(C3) <sub>3</sub>
empirical formula	TiC <sub>3</sub> H <sub>5</sub> O <sub>2</sub>	Li <sub>2</sub> TlC <sub>9</sub> H <sub>15</sub> O <sub>6</sub>
<i>M<sub>r</sub></i> (g·mol <sup>-1</sup> )	277.44	437.46
crystal system	orthorhombic	orthorhombic
space group (no.)	<i>Pca</i> 21 (29)	<i>P212121</i> (19)
crystal size (mm)	0.08 × 0.04 × 0.01	0.05 × 0.03 × 0.01
temperature (K)	298(2)	298(2)
<i>a</i> (Å)	7.3020(15)	4.9090(10)
<i>b</i> (Å)	10.636(2)	11.892(2)
<i>c</i> (Å)	21.028(4)	23.014(5)
<i>V</i> (Å <sup>3</sup> )	1633.1(6)	1343.5(5)
<i>Z</i>	12	4
<i>λ</i> (Å)	0.7513	0.9786
<i>D<sub>c</sub></i> (g·cm <sup>-3</sup> )	3.390	2.163
<i>μ</i> (mm <sup>-1</sup> )	32.946	17.265
reflection collected	2535	1135
reflections with <i>I</i> > 2σ( <i>I</i> )	1584	1035
parameters refined	165	165
hydrogen treatment	H-atom parameters not refined (geom.)	H-atom parameters not refined (geom.)
<i>R</i> -factor	0.0700	0.0520
<i>wR</i> -factor	0.2100	0.1316
goodness of fit	1.020	1.114
CCDC deposition numbers	770314	770315

**TABLE 2: Temperatures, Enthalpies, and Entropies of the Transitions of the Pure Compounds**

compound	transition	<i>T</i> /K	Δ <i>H</i> /kJ·mol <sup>-1</sup>	Δ <i>S</i> /J·mol <sup>-1</sup> ·K <sup>-1</sup>
LiC3	SII–SI <sup>a</sup>	549.7 ± 0.7	3.1 ± 0.1	5.6 ± 0.2
	SI–IL	606.4 ± 0.5	16.3 ± 0.2	26.9 ± 0.4
LiC5	SIII–SII	205.5 ± 0.5	1.31 ± 0.05	6.3 ± 0.3
	SII–SI	325.2 ± 0.7	3.0 ± 0.1	9.3 ± 0.3
TiC3	SI–IL	576.5 ± 0.3	21.74 ± 0.03	37.71 ± 0.07
	SIII–SII	278.3 ± 0.5	3.94 ± 0.05	14.2 ± 0.2
	SII–SI	365.8 ± 0.4	0.39 ± 0.04	1.0 ± 0.1
TiC5	SI–IL	466.6 ± 0.5	10.3 ± 0.1	22.1 ± 0.2
	SVI–SV	205.2 ± 0.4	0.40 ± 0.05	2.0 ± 0.3
	SV–SIV	219.2 ± 0.5	0.08 ± 0.04	0.4 ± 0.2
	SVI–SIII	234.3 ± 0.3	0.40 ± 0.05	1.7 ± 0.3
	SIII–SII	283.8 ± 0.3	2.41 ± 0.03	8.5 ± 0.1
	SII–SI	351.9 ± 0.3	1.96 ± 0.05	5.6 ± 0.2
	SI–LC	453.1 ± 0.5	5.92 ± 0.05	13.1 ± 0.2
	LC–IL	487.6 ± 0.4	3.36 ± 0.04	6.9 ± 0.1
Li <sub>2</sub> Tl(C3) <sub>3</sub> <sup>b</sup>	SII–SI	367.7 ± 0.3	4.9 ± 0.05	13.3 ± 0.2
	incongruent fusion	512.0 ± 0.7	41.9 ± 0.2	81.8 ± 0.4
Li <sub>2</sub> Tl(C5) <sub>3</sub> <sup>b</sup>	SII–SI	406.6 ± 0.5	8.0 ± 0.1	16.7 ± 0.2
	incongruent fusion	461.2 ± 0.3	24.3 ± 0.2	52.7 ± 0.5

<sup>a</sup> Referred to the S–S transition in the first heating of the LiC3. <sup>b</sup> Values referred to the mixed salts as pure compounds (the molecular weight of these salts is 3 times the average molecular mass weight of the mixtures with that composition).

the crystal phase structures, and their mesophases are still not explained. Other reasons to have chosen TiC<sub>*n*</sub> and LiC<sub>*n*</sub> for this study were also the presence of the condis phase in the TiC<sub>*n*</sub> series,<sup>37</sup> and a possible rotator phase in the LiC<sub>*n*</sub> series.<sup>44</sup> Moreover, a mixed salt with different-sized cations can allow the movement of the smallest one (Li), and an order–disorder transition could appear, accompanied by an increase of its electrical conductivity.

The aim of the present paper is to study the possible liquid-crystalline mesomorphism<sup>15,50</sup> in mixtures of nonthermotropic salts containing a common organic anion and two metallic cations, very different in size. In particular, we present a thorough study of the binary phase diagrams of lithium and thallium(I) propanoates and pentanoates over the whole composition range by means of DSC, XRD, FTIR, and polarizing light microscopy. A further target is to provide a good description of the mixed salts for both systems and of the liquid-crystal region in the case of the lithium and thallium(I)

*n*-pentanoates diagram. Special effort was paid to solve the crystal structures of the pure and mixed salts in order to infer information of their thermal behavior and properties.

## 2. Experimental Section

**2.1. Pure Components.** The thallium(I) salts were prepared by chemical reaction between the corresponding acids (propionic acid, Fluka, ≥ 99.5%, and valeric acid, Fluka, ≥ 99%), and thallium(I) carbonate (Riedel-de Haën, ≥ 99%), in methanol (Merck, ≥ 99.8%), being later recrystallized several times in an 1:1 ethanol/ether mixture (Merck, ≥ 99.8%, and Fluka, > 99.8%, respectively), and vacuum-dried.<sup>37,46</sup> LiC3 and LiC5 were prepared as described elsewhere.<sup>44</sup> Special attention was paid to the purity of all the samples to avoid the formation of acid soap or the presence of water.<sup>50–56</sup>

The purity was assessed by DSC, obtaining values of 99.72, 99.91, 99.97, and 99.98% for TiC3, TiC5, LiC3, and LiC5, respectively.

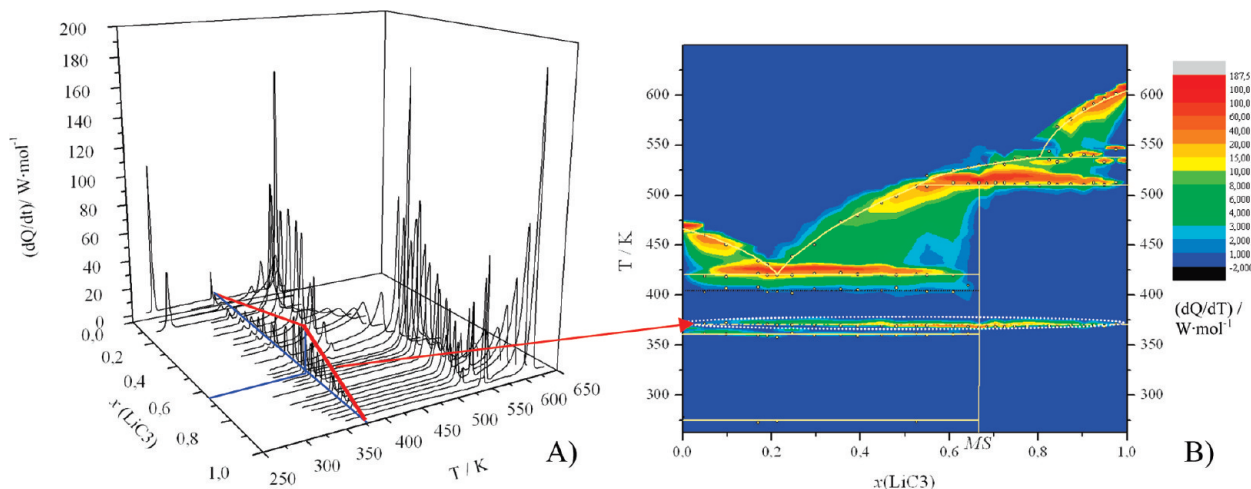


**Figure 1.** (A) 3D plot (heat flow vs composition vs temperature) for LiC3 + TIC3 system. (B) Contour plot (with  $z$  corresponding to the heat flow) of the diagram composition vs temperature.

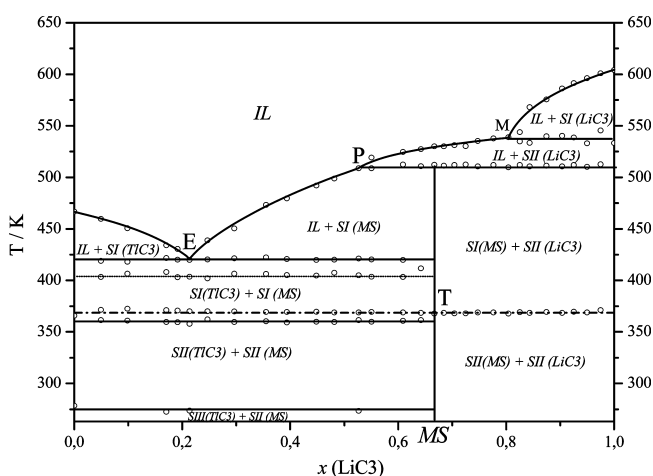


**Figure 2.**  $T$  vs composition plot for the LiC3 + TIC3 system, showing the eutectic (E) and the peritectic (P) points, and points T (solid-to-solid transition of the mixed salt), and M (joint of the two solubilizations of LiC3). IL, isotropic liquid; ILC, ionic liquid crystal; SN(TiC3), where  $N = I-III$ ,  $N$  solid phase of TiC3; SN(LiC3), where  $N = I-II$ ,  $N$  solid phase of LiC3.

Once the binary phase diagrams were solved, the mixed salts,  $\text{Li}_2\text{Tl}(\text{C}_3)_3$  and  $\text{Li}_2\text{Tl}(\text{C}_5)_3$ , were prepared in a different way, apart from the routes described above. Stoichiometric amounts (2:1) of LiC3 and TIC3, and of LiC5 and TIC5, respectively, were dissolved in hot ethanol. When the solution was cooled, a salt precipitated. In the case of  $\text{Li}_2\text{Tl}(\text{C}_5)_3$ , it was necessary to evaporate some ethanol from the solution. In both cases, the two salts were washed with acetone (Merck, > 99.5%) and vacuum-dried. The thermal behavior of the mixed salts thus obtained is similar to that of the mixtures with the same composition.

All the compounds here synthesized grow into flake-shaped crystals. Thus, crystallization produced very tiny crystals, whose sizes are given in Table 1. Crystals used for X-ray studies were grown by slow evaporation of the solvents from the solutions of compounds in ethanol and in ethanol/ether (1:1) for  $\text{Li}_2\text{Tl}(\text{C}_3)_3$  and TIC3, respectively.

**2.2. Mixed Salts and Mixtures Preparation.** In order to cover the whole composition range, 20 mixtures (of about 0.3 g each) were prepared by weighing the proper amounts of both components in Pyrex vials. Two methods for homogenization were used: (a) heating the mixtures until one of the components

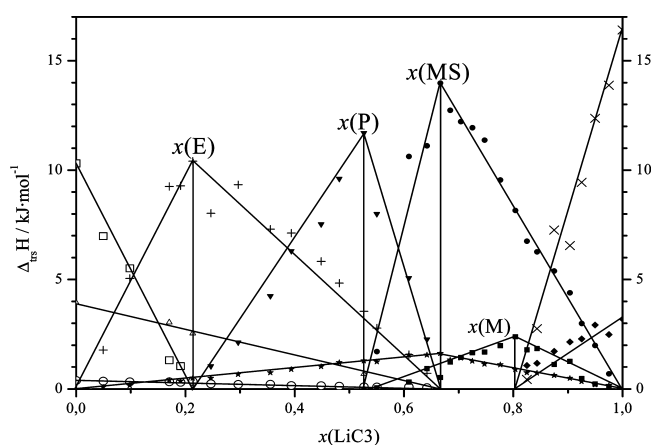


**Figure 3.**  $\Delta H$  (per mole of mixture) vs composition plot for the LiC3 + TIC3 system, for the transitions: (□) solubilization of the TIC3; (Δ) SIII-to-SII transition of TIC3; (○) SII-to-SI transition of TIC3; (+) eutectic reaction; (●) peritectic reaction; (▼) solubilization of the mixed salt (MS); (★) SII-to-SI transition of the mixed salt; (◆) SII-to-SI transition of the LiC3; (■) first solubilization of LiC3; (×) second solubilization of LiC3.

dissolved the other one, in inert atmosphere, followed by a solidification and grinding of the mixture (repeating at least 3 times this process),<sup>17,57</sup> and (b) dissolving the weighed samples in methanol (Merck, 99.8%), and then removing the solvent with a rotavapor; mixtures were finally high vacuum-dried, in order to get homogeneous and dried powdered samples.<sup>18</sup> The second method of homogenization is preferred as it avoids heating the samples repeatedly before running the DSC measurements, therefore getting a real first heating on the sample when measuring by DSC. In both cases, the estimated error in the molar fraction  $x$  was at most ( $\pm 0.002$ ). The two routes were followed to prepare the [LiC3 + TIC3] system, showing the same result, and only the second one was used for the [LiC5 + TIC5] system.

**2.3. Techniques. Differential Scanning Calorimetry.** A TA Instruments DSC, Model Q10, was used to register all the thermograms. Tightly sealed aluminum pans were used, in dry nitrogen, flowing at  $50.0 \text{ mL} \cdot \text{min}^{-1}$ . A MT5 Mettler microbalance was used to weigh the samples, ranging between 3 and 10 mg (with an error of  $\pm 0.001 \text{ mg}$ ). The calorimeter was calibrated in temperature using standard samples of In and Sn, supplied by TA (purity >99.999% and >99.9%, respectively), and of

benzoic acid (purity >99.97%), supplied by the former NBS (lot 39i), and in enthalpy with the In and Sn standards already described.

All the measurements were done at a heating rate of 5 K·min<sup>-1</sup>. All the scans were usually explored from 200 K to the temperature corresponding to the isotropic liquid in each case (a maximum of 650 K).

**Single-Crystal X-ray Diffraction (SCXRD).** Two crystal structures, for Li<sub>2</sub>Tl(C3)<sub>3</sub> and TIC3, were solved and refined by means of single-crystal diffraction. X-ray measurements were conducted using synchrotron radiation (with  $\lambda = 0.9786$  Å for Li<sub>2</sub>Tl(C3)<sub>3</sub>, and  $\lambda = 0.7513$  Å for TIC3) at the BM16 Spanish beamline of ESRF. Data sets of 360 images were collected in a ADSC-q210r CCD detector. The oscillation range ( $\Delta\varphi$ ) used for each image was 1°. Both salts were measured at room temperature.

The structures of these compounds are bilayered (ionic and lipidic alternating layers), as can be observed from the solved crystals. Thus, the joint between these latter layers is very weak, and it is of great difficulty to obtain good crystals due to the ease with which they exfoliate. The biggest single crystals obtained of these salts presented a size of 0.05 × 0.03 × 0.01 and 0.08 × 0.04 × 0.01 mm for Li<sub>2</sub>Tl(C3)<sub>3</sub> and TIC3, respectively. Furthermore, crystals for both compounds do not diffract beyond 0.9 Å, and also suffer severe radiation damage, specially TIC3, so the data presented a great intricacy to be treated, but they were still reliable enough to solve the structures.

The structures were solved by direct methods and subsequent Fourier syntheses using the SHELXS-97 program<sup>58</sup> and were refined by the full-matrix least-squares technique against  $F^2$  with the SHELXL-97 program,<sup>59</sup> in anisotropic approximation for all non-hydrogen atoms being all the parameters for the hydrogen atoms calculated geometrically in both compounds. An absorption correction was done for both crystals, due to the presence of heavy atoms. The main crystallographic data and some experimental details are shown in Table 1.

Further crystallographic details for the structures reported in this paper may be obtained from the Cambridge Crystallographic Data Center (see Supporting Information).

**Powder X-ray Diffraction.** High-resolution powder diffraction (HRPD) measurement was performed at SpLine beamline (BM25A) of the Spanish CRG at the European Synchrotron Radiation Facility (ESRF, Grenoble) with a fixed wavelength of 0.8266 ± 0.0001 Å, at room temperature. The powdered sample was placed inside a 0.5 mm diameter glass capillary, which was rotated during exposure. Data collection was done in a 2 $\theta$ -step scan mode with 0.015° step and 5 s acquisition time per point.

Routine powder XRD measurements were carried out with a Philips X'Pert PRO MPD X-ray diffractometer with vertical goniometer  $\theta/\theta$  (Cu K $\alpha$ 1 radiation, 1.540 56 Å, Ni filter), X'Celerator detector, equipped with a high-temperature chamber Anton Paar HTK1200. In situ XRD area was scanned from 2 $\theta$  = 2° to 70° at several temperatures in the range from 273 to 600 K during the heating and the cooling, at a rate of 3 °C/min.

**FTIR Spectroscopy.** Mid-infrared spectra of the samples as KBr pellets and powders between two pure KBr pellets were recorded at a resolution of 4 cm<sup>-1</sup> in a Nicolet Magna 750 FTIR spectrometer. No significant differences between the spectra obtained by both procedures were observed. A commercial variable-temperature cell, SPECAC VTL-2, adapted for solid samples was employed to obtain IR spectra at different temperatures.

**Optical Microscopy.** To identify the nature of the existing phases (solid, isotropic liquid, or liquid crystal phases), a Carl Zeiss-Jena polarizing optical microscope (model Jenalab Pol-30-G0527), equipped with a LINKAM hot stage (model THMS600) connected to a LINKAM programmable temperature-controller (model TMS94), was used.

### 3. Results

**3.1. Thermal Analysis. Pure Components.** The solid-to-solid transitions of LiC3, LiC5, TIC3, and TIC5 were studied by adiabatic calorimetry<sup>28,30,37</sup> and by DSC<sup>44,31,32,46</sup> in the super-ambient region (including here the melting and clearing processes). However, DSC thermograms were carried out again on the pure samples used in the present work to prepare all of the mixtures, which data are listed in Table 2, and are in fair agreement with the previously reported values.

**Binary Systems. (a) LiC3 + TIC3.** To study this phase diagram, a total of 29 mixtures of different molar fractions were prepared (by the two methods described in the Experimental Section). The output data obtained by DSC were normalized to "heat flow per mole of mixture" in order to make thermograms of different mixtures comparable with each other. Thus, a three-dimensional (3D) representation heat flow/temperature/molecular fraction (Figure 1A) could be built. The 2D projection of the former representation is also given in Figure 1B, showing the construction of the  $T$  vs  $x$  phase diagram. In order to make easier the construction of the phase diagram, only the pure TIC3 and two more mixtures were measured from 250 K just to confirm that the solid III-to-solid II transition of the pure salts appears as an invariant in the range  $0 \leq x(\text{LiC3}) < 0.667$ .

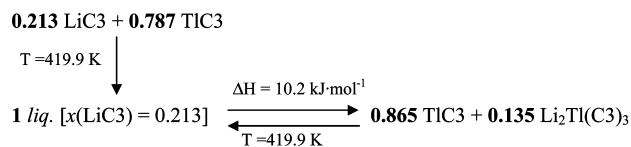
In Figure 2 the complete  $T$  vs  $x$  phase diagram is illustrated. In all the defined regions, except in the isotropic liquid (IL), two separated phases are observed.  $\Delta H$  vs  $x$  phase diagram (shown in Figure 3 for all of the reactions and characteristic points) has been developed following Tammann's method. This method is used commonly in the construction of the phase diagram to help in finding the characteristic points or invariants (isotherms), by plotting enthalpies (per mole of mixture) vs composition for each process (e.g., eutectic reaction).<sup>18,60</sup>

The characteristic reactions, eutectic and peritectic, in this binary system are given in Scheme 1.

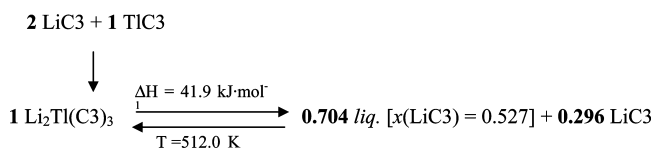
As can be appreciated (dotted line in Figure 2), a "premelting" effect appears just before the eutectic transition (as a small shoulder before the eutectic peak in these thermograms).

#### SCHEME 1: Description of the Eutectic and Peritectic Reactions for the LiC3 + TIC3 System<sup>a</sup>

**Eutectic reaction:**



**Peritectic reaction:**



<sup>a</sup> All of the phases are solid, except the ones indicated with liq. (liquid) with the corresponding composition of LiCn.

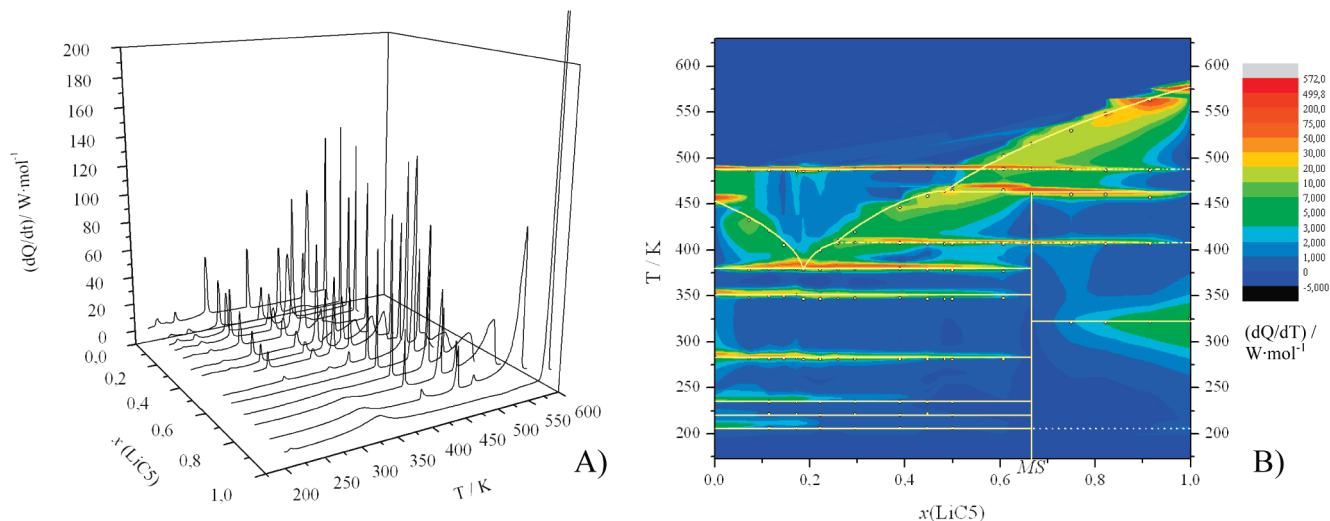


**Figure 4.** (A) 3D plot (heat flow vs composition vs temperature) for  $\text{LiC5} + \text{TIC5}$  system. (B) Contour plot (with  $z$  corresponding to the heat flow) of the diagram composition vs temperature.

The more significant process in this binary system is the formation of a mixed salt,  $\text{Li}_2\text{Tl}(\text{C3})_3$  (with a stoichiometry 2:1).  $\text{Li}_2\text{Tl}(\text{C3})_3$  has a solid-to-solid transition, SII-to-SI (point T and dash-dotted line in Figure 2), at 367.7 K (with an enthalpy of  $4.9 \text{ kJ} \cdot \text{mol}^{-1}$  per mole of mixed salt, or  $1.6 \text{ kJ} \cdot \text{mol}^{-1}$  per mole of mixture). Since the mixed salt is actually a pure compound, it is important to note that its molecular mass has to be 3 times the average molecular mass of the mixture with the composition  $x(\text{LiC3}) = 0.667$ , that is, 437.46 and  $145.82 \text{ g} \cdot \text{mol}^{-1}$ , respectively. The salt melts incongruently at 512.0 K as it is described in the peritectic reaction. The full thermal data for  $\text{Li}_2\text{Tl}(\text{C3})_3$  are shown in Table 2.

(b)  $\text{LiC5} + \text{TIC5}$ . This phase diagram was studied by preparing 20 different molar fractions, including the pure components, as explained in section 2.2. A 3D plot representing heat flow vs composition vs temperature of several mixtures and the corresponding contour plot constructing the phase diagram are shown in Figure 4, A and B, respectively.

The complete  $T$  vs  $x$  and  $\Delta H$  vs  $x$  phase diagrams are represented in Figures 5 and 6, respectively. All the defined regions, except in the isotropic liquid and the ionic liquid crystal (IL and ILC, respectively), correspond to two phase-separation regions, as explained for the  $\text{LiC3} + \text{TIC3}$  diagram. It is important to note that the transition SIII-to-SII of the  $\text{LiC5}$  could not be measured in the range of  $0.667 < x(\text{LiC5}) < 1$  due to the great undercooling of this phase change,<sup>44</sup> and so this transition is represented as a dotted line in Figure 5.

The characteristic reactions of this binary system, and also the eutectic and peritectic reactions, are described in Scheme 2.

A mixed salt with the composition (2:1) appears, as in the propanoate phase diagram. This compound was later isolated by crystallization in ethanol and studied by DSC.  $\text{Li}_2\text{Tl}(\text{C5})_3$  has a solid-to-solid transition, SII-to-SI (point T and dash-dotted line in Figure 5), and an incongruent fusion, as described in the peritectic reaction. The same considerations are taken for the molecular mass of this mixed salt, as in the case of the  $\text{Li}_2\text{Tl}(\text{C3})_3$ . The thermal data for the  $\text{Li}_2\text{Tl}(\text{C5})_3$  are also given in Table 2.

Besides the mixed salt, the most important feature in this binary system is the large interval of existence of an ionic liquid-crystal phase (ILC): from  $x(\text{LiC5}) = 0$  to 0.56, point M in Figure 5. The existence of this phase extends as well from 35 K in the

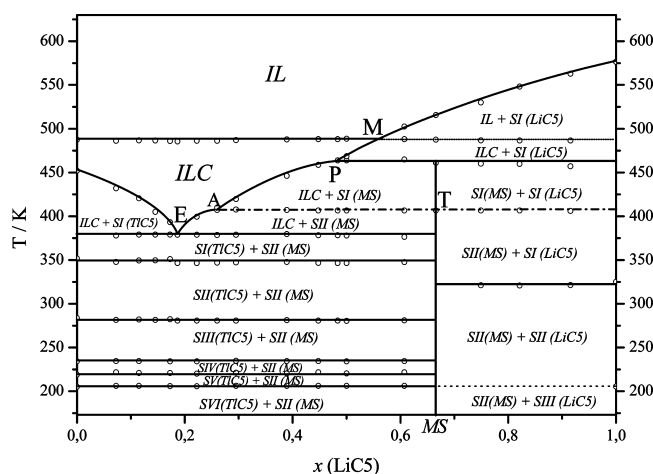


**Figure 5.**  $T$  vs composition plot for the  $\text{LiC5} + \text{TIC5}$  system, showing the eutectic (E) and the peritectic (P) points, and points T (solid-to-solid transition of the mixed salt), A (joint of the two solubilizations of the mixed salt), and M (joint of the clearing reaction with the solubilization of  $\text{LiC5}$ ). IL, isotropic liquid; ILC, ionic liquid crystal; SN(TiC5), where  $N = \text{I-VI}$ ,  $N$  solid phase of TIC5; SN(LiC5), where  $N = \text{I-II}$ ,  $N$  solid phase of  $\text{LiC5}$ .

pure TIC5 to 110 K in the eutectic mixture ( $x(\text{LiC5}) = 0.19$ ). It is remarkable that the fact of finding the clearing reaction of this ILC phase as an invariant that was not detected in similar phase diagrams reported.<sup>17,18</sup> This indicates the high stability of the liquid-crystal phase in the binary diagram.

Polarizing light microscopy was used to identify the liquid-crystal phase as “smectic A-like” or neat phase. In Figure 7, the typical focal conic domain of a neat phase is shown.

**3.2. Structural Analysis of Pure and Mixed Salts.** The structures of TIC3 and  $\text{Li}_2\text{Tl}(\text{C3})_3$  (by SCXRD) and of  $\text{Li}_2\text{Tl}(\text{C5})_3$  (by HRPD) were solved in this work. The expected bilayered arrangement is the main common feature in every compound, but a great difference in the packing of the ionic layer (and subsequently in the alkyl chains) was found.

TIC3 was measured at 298 K (SII phase) and presents an orthorhombic cell in the  $Pca21$  space group, shown in Figure 8A. Three slightly different thallium(I) cations are found, but sharing the same characteristics: they are coordinated by 6 oxygen atoms with a trigonal prism geometry, which results to be hemidirected, the thallium being in the same plane as four of these oxygen atoms (see Figure 8B).

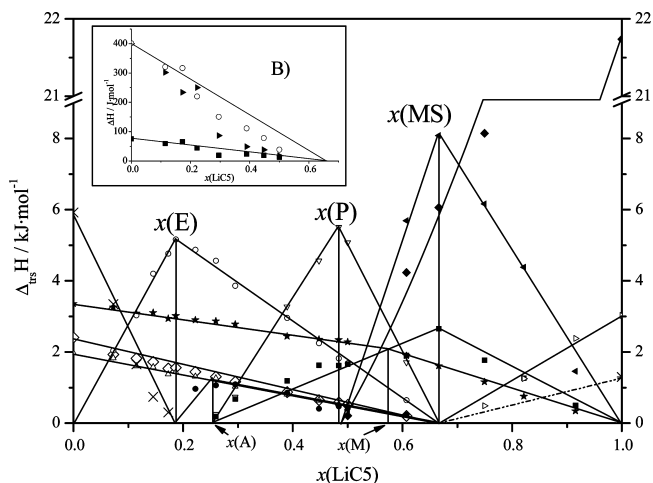
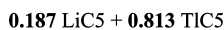


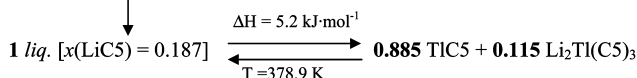
**Figure 6.**  $\Delta H$  (per mole of mixture) vs composition plot for the LiC5 + TIC5 system, for the following main transitions: (x) solubilization of TIC5; (★) clearing of the ILC phase; (◇) SIII-to-SII transition for TIC5; (Δ) SII-to-SI transition for TIC5; (○) eutectic reaction; (solid left-pointed triangle) peritectic reaction; (●) first solubilization of the mixed salt; (▽) second solubilization of the mixed salt; (■) SII-to-SI transition of the mixed salt; (open right-pointed triangle) SII-to-SI transition of LiC5; (◆) solubilization of LiC5. In the inset B, solid right-pointed triangle, ■, and ○ represent SVI–SV, SV–SIV, and SIV–SIII transitions for TIC5.

## SCHEME 2: Description of the Eutectic and Peritectic Reactions for the LiC5 + TIC5 System<sup>a</sup>

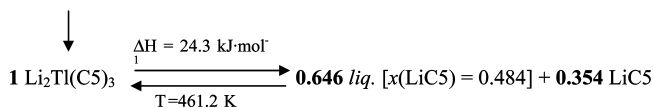
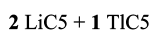
### Eutectic reaction:



$$T = 378.9 \text{ K}$$



### Peritectic reaction:



<sup>a</sup> All of the phases are solid, except the ones indicated with “liq.” (liquid) with the corresponding composition of LiC<sub>n</sub>.

The crystal for Li<sub>2</sub>Tl(C3)<sub>3</sub> corresponds to the low-temperature crystalline phase (SII) and presents an orthorhombic unit cell, with symmetry *P212121*. The structure presents two bilayers per unit cell, as can be seen in Figure 8A. The coordination of the lithium cations is tetrahedral, as in the pure lithium alkanates, while, in the case of the thallium atom, four O atoms coordinate it in a pyramidal geometry, the thallium being in apical position (see Figure 9B). There are other oxygens surrounding the Tl atom, but at distances longer than 3.25 Å, which is considered the limiting distance for a Tl–O bond in the literature.<sup>61</sup> Crystal data for these two salts are given in Table 1.

The structure for Li<sub>2</sub>Tl(C5)<sub>3</sub> was solved by HRPD and by Monte Carlo methods, and refined by means of the Rietveld method.<sup>62</sup> Reflection positions of the first 20 peaks were determined using the WinPLOTR<sup>63</sup> program and peak indexing was carried out with the DicVOL06<sup>64</sup> program, finding a monoclinic cell. Expo2004<sup>65</sup> program was used to find the space

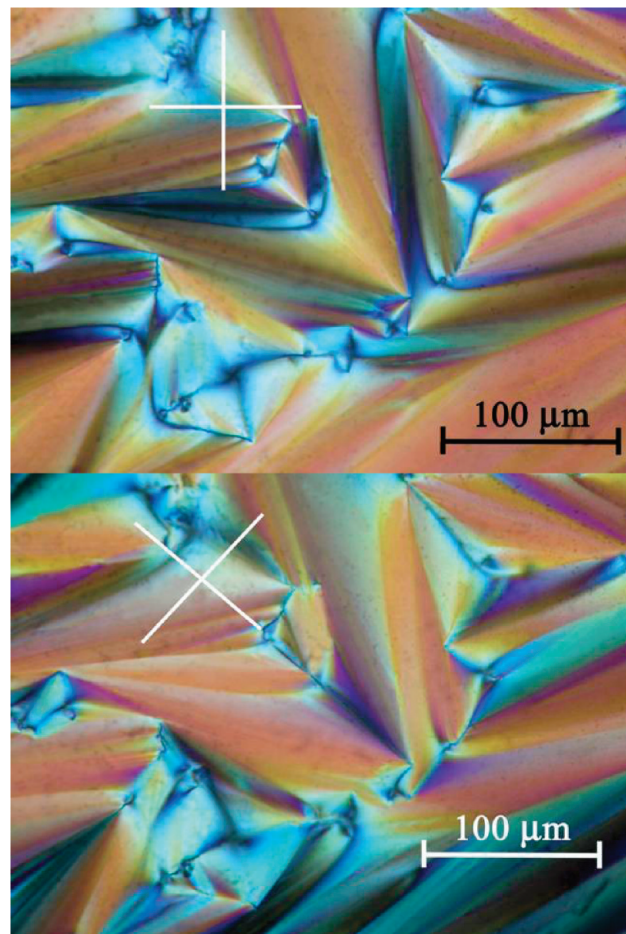


**Figure 7.** Typical fan shape domains of a “smectic A-like” (or neat phase). White crosses in the corners shows the orientation of the crossed polars. Pictures taken on a sample of  $x(\text{LiC5}) = 0.19$  (eutectic mixture) at 460 K.

group; after an automatic intensity extraction procedure, the statistical algorithm for finding the correct space group<sup>66</sup> found, as the most probable, the *P2<sub>1</sub>/c* extinction group.

Structure solution, by means of Direct Methods, was attempted with the Expo2004 program, within the *P2<sub>1</sub>/c* space group, without success. Thus, a new and successful attempt was carried out, this time using the Monte Carlo technique, with the FOX<sup>67</sup> program.

Atomic coordinates found by FOX were introduced in the FullProf<sup>68</sup> program in order to perform a Rietveld refinement; the atomic coordinates of the 24 independent non-H atoms were fitted, but solid rigid constraints on two parts of the alkyl chains were applied to limit the number of free parameters. Two different isotropic temperature factors were introduced: one for the Tl and one for the rest of atoms.

Crystal data for this compound can be found in Table 3, while in Figure 10 the result of the Rietveld refinement is shown.

Despite belonging to different crystal systems, the molecular arrangement is practically the same as in the case of Li<sub>2</sub>Tl(C3)<sub>3</sub>, principally in the ionic layer (see Figure 11). Thus, the only significant and logical difference is the increase in the *d*-spacing from Li<sub>2</sub>Tl(C3)<sub>3</sub> to Li<sub>2</sub>Tl(C5)<sub>3</sub>.

The *d*-spacings of the bilayers for the initial compounds and the mixed salts were also analyzed as a function of the temperature and are shown in Figure 12, indicating the different ordered phases and reactions. A decrease in the *d*-spacing in the SII–SI transitions, which will be discussed later, and the

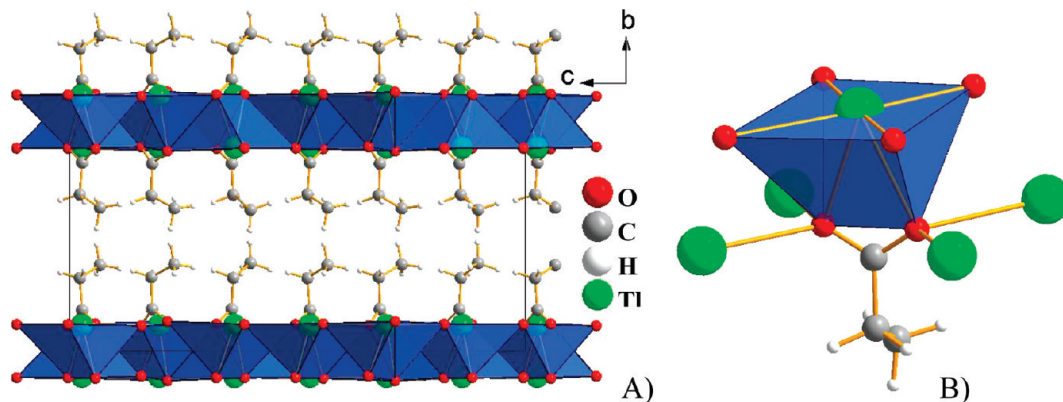


**Figure 8.** (A) Crystal structure for the TIC3 in the *bc* projection. (B) Coordination of the thallium atoms in a trigonal prism geometry.

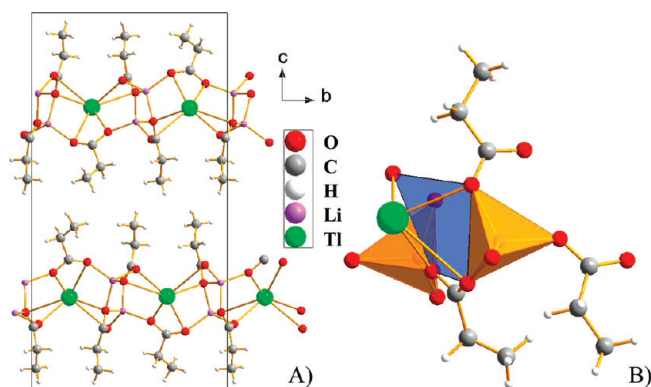


**Figure 9.** (A) Crystal structure for the  $\text{Li}_2\text{Tl}(\text{C}_3)_3$  in the *bc* projection. (B) Coordination of the lithium (tetrahedral) and thallium atoms (pyramidal geometry, with thallium in apical position).

decomposition in the peritectic reaction are clearly detected for both mixed salts. In the case of the  $\text{Li}_2\text{Tl}(\text{C}_5)_3$ , the ILC and the  $\text{SI}(\text{LiC}_5)$  phases, both ordered phases, coexist after this peritectic reaction.

**3.3. FTIR Spectroscopy.** A FTIR study as a function of temperature was carried out for  $\text{Li}_2\text{Tl}(\text{C}_3)_3$ ,  $\text{Li}_2\text{Tl}(\text{C}_5)_3$ , TIC3, and TIC5 in order to study structural changes at the different phase transitions. The infrared spectra recorded for  $\text{Li}_2\text{Tl}(\text{C}_5)_3$  at room temperature (SII) and after the solid-to-solid transition (SI) are displayed in Figure 13A. Three bands corresponding to the asymmetric vibrations of coordinate carboxylate groups ( $\nu_{\text{as}}(\text{COO})$ ) appear at 1582, 1560, and 1545  $\text{cm}^{-1}$  in the crystal at room temperature, according to the three different types of coordination detected by XRD, but only two of them at 1578 and 1556  $\text{cm}^{-1}$  are observed in the high-temperature solid phase, SI. The corresponding components for the  $\nu_{\text{s}}(\text{COO})$  symmetric stretching vibration are measured at 1449, 1436, and 1410  $\text{cm}^{-1}$  in the SII, and at 1436 and 1410  $\text{cm}^{-1}$  in the SI. The difference in wavenumbers between these vibrations is related to the type of carboxylate-to-metal coordination present in the salt. In this compound, such difference is between 146 and 138  $\text{cm}^{-1}$  which is consistent with the bridging and chelating coordination determined by X-ray data. The frequency of bands corresponding to methyl group deformation and methylene wagging and rocking vibrations is constant with temperature; only broadening of these bands is observed as a consequence of the temperature increase. This would imply that the all-trans order is present in both phases, SII and SI.

The methyl and methylene stretching vibrations region is displayed in Figure 13B. The symmetric stretching band corresponding to the  $\text{CH}_3$  group shifts from 2955  $\text{cm}^{-1}$  in SII to 2960  $\text{cm}^{-1}$  in SI. This frequency shift must be related to

intermolecular end chain interactions that are different in the two solid phases. This is consistent with the shortening observed by powder XRD in the *d*-spacing from SII to SI. No bands corresponding to the acid in any of the samples are observed, which shows the high purity of both samples.

#### 4. Discussion

The main feature of the  $\text{LiC}_3$ –TIC3 and  $\text{LiC}_5$ –TIC5 phase diagrams is the formation of a mixed salt, which occurs at the same composition (2:1) in both systems. The molecular packing is the same in both mixed salts: a bilayered arrangement of ionic (lithium, thallium, and carboxylate ions) and lipidic (alkyl chains) planes. Consequently, the existence of a mixed dilithium and thallium(I) alkanooates series,  $\text{Li}_2\text{Tl}(\text{C}_n)_3$ , can be predicted, since the growth of the alkyl chain does not affect to the ionic packing.

Apparently, no significant differences are found when comparing the room temperature crystalline structure of the pure and mixed salts. However, despite all of them presenting a bilayered packing, their ionic arrangement differs enough to enable or disable the movements in the alkyl chains. This fact can be quantified with the value of the cross-sectional area of the alkyl chains ( $S'$ ), that is, the space that the alkyl chain has to be able to form gauche defects. This parameter depends on the area per polar head ( $S$ ),<sup>69</sup> and on the torsion (tilt) of the plane of the chains with respect to the ionic plane ( $\alpha$ ), with this relation:  $S' = S \cos(\alpha)$ . The torsion is almost negligible for TIC3 (4–6°), and for  $\text{Li}_2\text{Tl}(\text{C}_3)_3$  and  $\text{Li}_2\text{Tl}(\text{C}_5)_3$ , since they have two of the three chains with 2 and 6° of tilt. In the case of  $\text{LiC}_3$  and  $\text{LiC}_5$   $\alpha$  is 33°. The values of  $S$  (and  $S'$ , if necessary) are 25.6 Å<sup>2</sup> for TIC3; 19.5 and 19.7 Å<sup>2</sup> for  $\text{Li}_2\text{Tl}(\text{C}_3)_3$  and  $\text{Li}_2\text{Tl}(\text{C}_5)_3$ , respectively; and 21.4 (18.6) and 21.8 (18.7 Å<sup>2</sup>), for  $\text{LiC}_3$  and  $\text{LiC}_5$ , respectively. From these results, it is clear to infer the more packed arrangement in the cases of the lithium and mixed alkanooates than for the thallium salts. The structure of the thallium(I) alkanooates was studied previously by Dorfler et al.,<sup>47,48</sup> giving values of around 24 Å<sup>2</sup> for  $S$ , for longer members of the series, comparable with the one found in this work for the TIC3. This great value of  $S$  (and  $S'$ ) explains the presence of disorder in the chains of the thallium(I) alkanooates at room temperature, observed by FTIR, forming the so-called “condis” phase (solid phase where the alkyl chains are conformationally disordered), already studied.<sup>37,49</sup> It also fits perfectly with the difficulty in obtaining good results in the X-ray study (in single crystal and in powder) of the ionic layer structure in the compounds of the TIC<sub>*n*</sub> series when  $n \geq 4$ : the single-crystalline flakes were found to be “plastic”, and easily bendable. The order gets lost in the ionic plane, being only clearly visible

**TABLE 3: Crystallographic Data, Experimental Parameters and Structure Refinement Data for  $\text{Li}_2\text{Tl}(\text{C5})_3$** 

Crystal Data	
formula	$\text{Li}_2\text{TlC}_{15}\text{H}_{27}\text{O}_6$
$M_r$ ( $\text{g}\cdot\text{mol}^{-1}$ )	521.67
cell setting, space group (no.)	monoclinic, $P2_1/c$ (14)
temperature (K)	298(2)
$a, b, c$ ( $\text{Å}$ ), $\beta$ (deg)	4.92113(7), 12.0299(2), 33.8176(5), 91.3463(12)
volume ( $\text{Å}^3$ )	2001.46(5)
$Z, D_c$ ( $\text{g}\cdot\text{cm}^{-3}$ )	4, 1.6402
wavelength ( $\text{Å}$ )	0.8266(1)
$\mu$ ( $\text{mm}^{-1}$ )	3.75
Data Collection	
diffractometer	Spline (BM25A) at the ESRF, Grenoble
specimen mounting	borosilicate glass capillary
data collection mode	transmission
scan mode	$2\theta$ -step scan
$2\theta$ range (deg), step size ( $2\theta$ deg)	1–50, 0.015
Refinement	
refinement method	full-matrix least-squares on $I_{\text{net}}$
$R_p, R_{\text{wp}}, R_{\text{exp}}$	0.00964, 0.0138, 0.0136
$R_F, R_{\text{BRAGG}}$	0.0267, 0.0353
goodness-of-fit	1.901
profile function	pseudo-Voigt with axial divergence asymmetry
no. of contributing reflections	2217
no. of parameters	96
no. of rigid bodies	6
CCDC deposition no.	770316

the  $d$ -spacing between bilayers. This value of  $S$  can also explain the great thermal agitation found in the O and C atoms in the TIC3, where the carboxylate anions could rotate perpendicularly to the Tl planes.

Thallium(I) is comparable in size and in charge with some alkaline cations, such as potassium and cesium. A similar trigonal prism coordination (6 coordinating oxygen atoms), is found for some potassium alkanooates,<sup>70,71</sup> with the only difference that the potassium cation is inside the prism in these cases, instead of in its base, as it occurs with the thallium(I) in the TIC3 (hemidirected coordination). This makes the value of  $S$  for TIC3 ( $25.6 \text{ Å}^2$ ) larger than the one for KC10 ( $22.9 \text{ Å}^2$ ). The packing changes significantly for cesium carboxylates, which present a cubic coordination (by 8 oxygen atoms) and a  $S$  of  $22.2 \text{ Å}^2$ .<sup>72</sup>

One solid-to-solid transition was found for both dilithium and thallium(I) mixed salts. The nature of this phase transition may be explained by the different techniques used here. The ionic

arrangement was found to be the same for both salts, the difference in the chain length being the only possible reason for the difference in the transition enthalpy found by DSC, which increases with the alkyl chain length. Moreover, the FTIR study shows that the order in the all-trans conformation is maintained also in the high-temperature phase (SI). These results point that the SI could be a rotator phase, as it happens in the lithium and in the lead(II) alkanooates.<sup>44,69,73,74</sup>

Besides the formation of the mixed salts, these binary systems give information about the existence and/or the stabilization of an ionic liquid-crystal phase (ILC) as a homogeneous region in the binary phase diagram. On the one hand, when mixing organic salts with different-sized metal cations, mesogenicity is favored, and, at the same time, its thermal stability,<sup>15</sup> which is the case for the LiC5–TlC5 binary system. On the other hand, there is a critical length for the alkyl chain to form ILC phases, similarly to what happens for pure metal alkanooates series.<sup>5</sup>

While no liquid-crystalline phase is observed in the LiC3–TlC3 phase diagram, a broad and greatly stabilized ILC phase is found

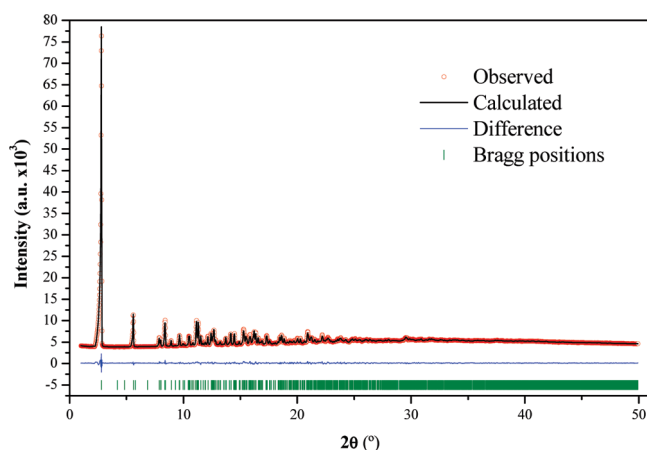


**Figure 10.** Rietveld refinement for the  $\text{Li}_2\text{Tl}(\text{C5})_3$ , comparing the observed and calculated diffraction patterns, their difference, and Bragg positions.

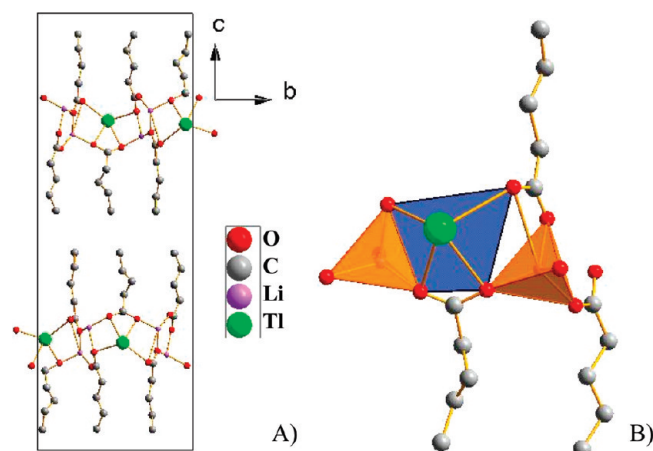


**Figure 11.** (A) Crystal structure for the  $\text{Li}_2\text{Tl}(\text{C5})_3$  in the  $bc$  projection. (B) Coordination of the lithium (tetrahedral) and thallium atoms (pyramidal geometry, with thallium in apical position).

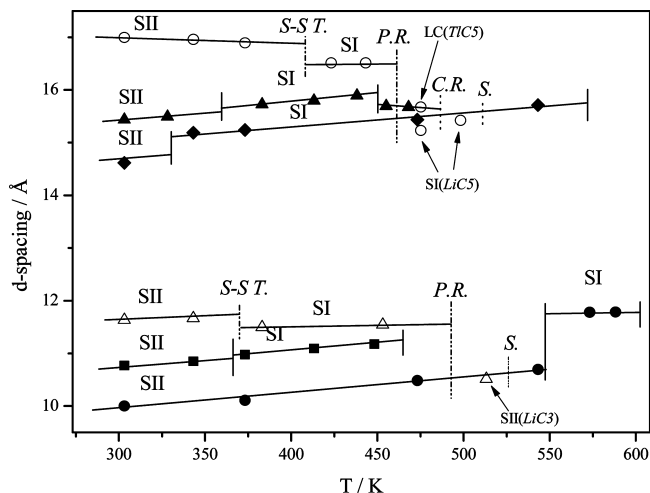


**Figure 12.** *d*-spacing vs temperature indicating the different phases, for (●) LiC<sub>3</sub>, (■) TIC<sub>3</sub>, (△) Li<sub>2</sub>Tl(C<sub>3</sub>)<sub>3</sub>, (◆) LiC<sub>5</sub>, (▲) TIC<sub>5</sub>, and (○) Li<sub>2</sub>Tl(C<sub>5</sub>)<sub>3</sub>. In the case of the mixed salts, the reactions are displayed with dash-dotted lines, where S–S T. = solid-to-solid transition, P.R. = peritectic reaction, C.R. = clearing reaction, and S. = solubilization. The resulting compounds after the incongruent melting of the mixed salts (peritectic reactions) are also indicated.

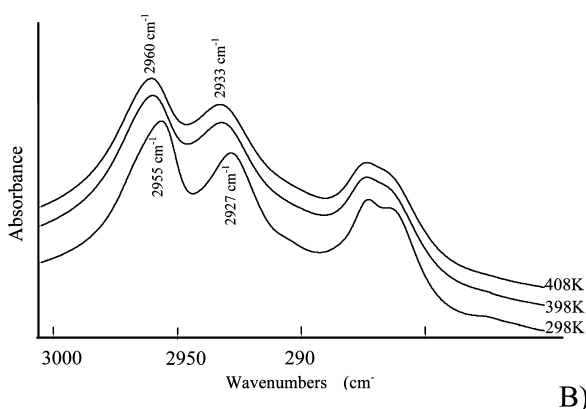
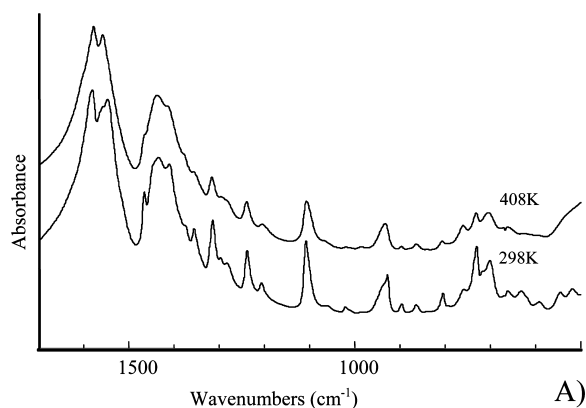


**Figure 13.** FTIR spectra for Li<sub>2</sub>Tl(C<sub>5</sub>)<sub>3</sub> (A) in the  $\nu(\text{COO})$  region at  $T = 298$  and  $408$  K, and (B) in the  $\nu(\text{CH})$  region at  $T = 298$ ,  $398$ , and  $408$  K.

in the LiC<sub>5</sub>–TlC<sub>5</sub> system. Thus, the temperature range of existence of the ILC phase extends from 35 to 108 K, from the pure TIC<sub>5</sub> to the eutectic composition, since the clearing points remain as an invariant (see section 3.1). Moreover, the temperature of appearance of the ILC decreases to 419.9 K in the eutectic composition, which is a very low temperature for molten

metal soaps.<sup>75</sup> Comparing both binary systems, the effect of the chain length becomes clearly crucial in the formation of the ILC phases.

A comparison between the LiC<sub>3</sub>–TlC<sub>3</sub> and the LiC<sub>3</sub>–CsC<sub>3</sub> systems<sup>17</sup> will be useful in order to find what the influence of the different cations is, maintaining the same chain length. The former does not exhibit a mesogenic phase, but the latter surprisingly does, even when none of the pure compounds is mesogenic, showing that the different nature of the cation plays a basic role in mesogenicity. The chain length and cation size dependence have been deeply studied in several metal alkanolate series for the appearance of liquid-crystal phases.<sup>5,6,13,14</sup> Taking into account only the monovalent metal alkanolate series, the appearance of the liquid-crystal phase starts from  $n \geq 4$  for NaCn and KCn, from  $n \geq 5$  for RbCn and TlCn, from  $n \geq 6$  for CsCn, and from  $n \geq 12$  for LiCn,<sup>5,6</sup> (being  $n$  the total number of carbon atoms of the shortest member forming this mesophase, or critical length). In this sense, we may consider these lithium and thallium alkanolate systems, LiCn–TlCn, as a series itself, and compare it with those series. The formation of an ionic liquid-crystal phase can be interpreted on the basis of the size and polarizability of the cations. Thus, the series with intermediate-sized cations presents a ILC phase with lower values of  $n$ , 0.59, 1.02, 1.38, 1.52, 1.67, and 1.50 Å being the ionic radii for monovalent Li, Na, K, Rb, Cs, and Tl, respectively.<sup>76</sup> This agrees with the LiC<sub>4</sub>–RbC<sub>4</sub> phase diagram, which presents an ILC phase, and where  $n$  decreases from 5 and 12 (for RbCn and LiCn, respectively) to 4 (in this binary system).<sup>18</sup> This is the same case for the LiC<sub>3</sub>–CsC<sub>3</sub> system. According to that, the formation of the ILC phase may be also more favored in the LiCn–TlCn systems than in pure LiCn and TlCn, but this phase seems to start with  $n = 5$ , as in the TICn series. However, the stability of this mesophase is greatly improved in the phase diagrams. It is important to remark the low polarizability of thallium ion, which forms less ionic and weaker bonds than the alkaline ions. This could be the reason why  $n$  does not decrease from the TICn series ( $n = 5$ ) to the LiCn–TlCn systems and it does in the case of binary systems with alkaline atoms. That also explains the lower melting points of thallium(I) alkanolates in comparison with those of the alkaline ones.

## 5. Conclusions

The phase diagrams of the lithium and thallium(I) propanoate and pentanoates have been thoroughly studied by DSC, XRD, FTIR, and polarizing light microscopy, in the temperature range from 200 K up to the temperatures of existence of the isotropic liquid phase.

Similarities were found in the two phase diagrams studied. The existence of a mixed salt with a composition of 2:1 (in the lithium:thallium(I) ratio) has been demonstrated. The two mixed salts, Li<sub>2</sub>Tl(C<sub>3</sub>)<sub>3</sub> and Li<sub>2</sub>Tl(C<sub>5</sub>)<sub>3</sub>, have a similar arrangement of the ions in the ionic layers, the chain length being the only difference. They have been synthesized and characterized here for the first time. Furthermore, it has been proved that it is possible to obtain them by crystallization. Their thermal behavior is quite similar: both salts present a solid-to-solid transition, from crystal to a rotator phase, previous to their incongruent melting point. Similarly to the pure metal alkanolates series, the mixed salts constitute a series as well: dilithium and thallium(I) alkanolates.

The stabilization of the ILC phase, which was the initial desired feature, was found for the pentanoates phase diagram but not for the propanoates. Once again, the dependence on the alkyl chain becomes crucial for the existence of an ionic liquid-

crystalline phase. In the pentanoates binary system, the range of existence of the ILC phase increases from 35 K, in the pure TIC5, to 108 K in the eutectic mixture, showing the stabilization when mixing salts with different sized metal cations, as predicted by Mirnaya et al.<sup>15</sup> In this sense, ILC phases with low melting points can be used to prepare “ordered solvents” for selective reactions (“tailor-made” solvents). The liquid-crystal phase studied here cannot be considered as a “green solvent” because of the presence of thallium cation, but there is no doubt that it will help to establish correlation rules to find such kind of materials.

Besides lithium propanoate and pentanoate, previously studied by us,<sup>44</sup> three new crystalline structures were also analyzed, allowing us to study the complex polymorphism in these organic salts. As can be inferred from this work, there is a direct dependence between the cross-sectional area of the alkyl chains and their ability to show chain defects in the different polymorphic or mesomorphic states, which form the stepwise melting process, typical of all the organic salts. The cross-sectional area is a fundamental parameter to study in depth mesomorphic phases, such as rotator or condis, which currently are not well characterized.

**Acknowledgment.** Partial support of this research by the Beca de Especialización en Organismos Internacionales (ES-2006-0024) and by the DGICYT of the Spanish Ministerio de Ciencia e Innovación (Project CTQ2008-06328/BQU) are gratefully acknowledged. The authors thank BM16-LLS and BM25 (both Spanish beamlines at the ESRF, in Grenoble, France) and the CAIs (Centro de Asistencia a la Investigación) of XRD and Spectroscopy of the UCM for the use of their technical facilities.

**Supporting Information Available:** The structures reported in this paper may be obtained from the Cambridge Crystallographic Data Center, on quoting the depository numbers 770314, 770315, and 770316, for TIC3, Li<sub>2</sub>Tl(C3)<sub>3</sub>, and Li<sub>2</sub>Tl(C5)<sub>3</sub>, respectively. This material is available free of charge via the Internet at <http://pubs.acs.org>.

## References and Notes

- Ryckaert, J. P.; Klein, M.; McDonald, I. R. *Mol. Phys.* **1994**, *83*, 439–458.
- Marbeuf, A.; Brown, R. *J. Chem. Phys.* **2006**, *124* (5), 054901/1–054901/9.
- Wunderlich, B.; Möler, M.; Grebowicz, J.; Baur, H. *Conformational Motion and Disorder in Low and High Molecular Mass Crystals*; Höcker, H., Ed.; Advances in Polymer Science, No. 87; Springer-Verlag: Heidelberg, Germany, 1988.
- Vorländer, D. *Ber. Dtsch. Chem. Ges.* **1910**, *43*, 3120–3135.
- Franzosini, P.; Sanesi, M. *Thermodynamic and transport properties of organic salts*; Pergamon Press: Oxford, UK, 1980.
- (a) Skoulios, A.; Luzzati, V. *Acta Crystallogr.* **1961**, *14*, 278–286. (b) Gallot, B.; Skoulios, A. *Acta Crystallogr.* **1962**, *15*, 826–831. (c) Abied, H.; Guillon, D.; Skoulios, A.; Weber, P.; Giroud-Codquin, A. M.; Marchon, J. C. *Liq. Cryst.* **1987**, *2* (3), 269–279.
- Giroud-Godquin, A. M. *Handbook of Liquid Crystals*; Demus, D., Goodby, J., Gray, G. W., Spiess, K. W., Vill, V., Eds.; Wiley-VCH: Weinheim, Germany, 1998; Vol. 2B, Chapter XIV, p 901.
- Polishchuk, A. P.; Timofeeva, T. V. *Russ. Chem. Rev.* **1993**, *62*, 291–321.
- Hudson, S. A.; Maitlis, P. M. *Chem. Rev.* **1993**, *93*, 861–885.
- Mirnaya, T. A.; Prisyazhnyi, V. D.; Shcherbakov, V. A. *Russ. Chem. Rev.* **1989**, *58*, 1429–1450.
- Binnemans, K. *Chem. Rev.* **2005**, *105*, 4148–4204.
- Donnio, B. *Curr. Opin. Colloid Interface Sci.* **2002**, *7*, 371–394.
- Donnio, B.; Guillon, D.; Deschenaux, R.; Bruce, D. W. *Metal-lobesogens, In Comprehensive Coordination Chemistry II*; McCleverty, J. A., Meyer, T. J., Eds.; Elsevier: Oxford, UK, 2003; Vol. 7, Chapter 7.9, pp 357–627.
- Binnemans, K.; Görlner-Walrand, C. *Chem. Rev.* **2002**, *102*, 2303–2345.
- Mirnaya, T. A.; Volkov, S. V. *Ionic Liquid Crystals as Universal Matrices (Solvents). Main Criteria for Ionic Mesogenicity. In General Industrial Applications of Ionic Liquids*; Rogers, R. D., et al., Eds.; NATO Science Series; Kluwer Academic Publishers: Amsterdam, 2003; pp 439–456.
- Franzosini, P.; Ferloni, P. *Molten Alkali Metal Alkanoates*; Schiraldi, A., Spinolo, G., Eds.; IUPAC Solubility Data Series; Pergamon Press: Oxford, UK, 1988; Vol. 33.
- Mirnaya, T. A.; Yaremchuk, G. G.; Prisyazhnyi, V. D. *Liq. Cryst.* **1990**, *8*, 701–705.
- Martínez Casado, F. J.; Ramos Riesco, M.; Cheda, J. A. R. *J. Therm. Anal. Calorim.* **2007**, *87* (1), 73–77.
- Boerio-Goates, J.; López de la Fuente, F. L.; Cheda, J. A. R.; Westrum, E. F. *J. Chem. Thermodyn.* **1985**, *17* (5), 401–408.
- Ngeyi, S. P.; Westrum, E. F.; López de la Fuente, F. L.; Cheda, J. A. R.; Fernández Martín, F. *J. Chem. Thermodyn.* **1987**, *19* (3), 327–335.
- Ngeyi, S. P.; López de la Fuente, F. L.; Cheda, J. A. R.; Fernández Martín, F.; Westrum, E. F. *J. Chem. Thermodyn.* **1985**, *17* (5), 409–418.
- López de la Fuente, F. L.; Cheda, J. A. R.; Fernández Martín, F.; Westrum, E. F. *J. Chem. Thermodyn.* **1988**, *20* (10), 1137–1148.
- Ngeyi, S. P.; Westrum, E. F.; López de la Fuente, F. L.; Cheda, J. A. R.; Fernández Martín, F. *J. Chem. Thermodyn.* **1987**, *19* (12), 1261–1270.
- Labban, A. K.; López de la Fuente, F. L.; Cheda, J. A. R.; Westrum, E. F.; Fernández Martín, F. *J. Chem. Thermodyn.* **1989**, *21* (4), 375–384.
- López de la Fuente, F. L.; Cheda, J. A. R.; Jones, L. L.; Lin, C. C.; Westrum, E. F. *J. Chem. Thermodyn.* **1994**, *26* (9), 925–940.
- Cheda, J. A. R.; Ungarelli, P.; López de la Fuente, F. L.; Fernández Martín, F.; Xu, H. Y.; Ijdo, W. L.; Westrum, E. F. *Thermochim. Acta* **1995**, *266*, 163–173.
- Cheda, J. A. R.; Fernández Martín, F.; Burns, R. J.; Westrum, E. F. *J. Chem. Thermodyn.* **1994**, *26* (8), 829–838.
- Franzosini, P.; Westrum, E. F. *J. Chem. Thermodyn.* **1984**, *16* (2), 81–90.
- Franzosini, P.; Ngeyi, S. P.; Westrum, E. F. *J. Chem. Thermodyn.* **1986**, *18* (7), 609–618.
- Franzosini, P.; Ngeyi, S. P.; Westrum, E. F. *J. Chem. Thermodyn.* **1986**, *18* (12), 1169–1181.
- Sanesi, M.; Ferloni, P.; Franzosini, P. *Z. Naturforsch.* **1977**, *32a*, 1173–1177.
- Lindau, J.; Diele, S.; Kruger, H.; Dorfler, H. D. *Z. Phys. Chem.-Leipzig* **1981**, *262* (5), 775–784.
- Lindau, J.; König, H. J.; Dorfler, H. D. *Colloid Polym. Sci.* **1983**, *261* (3), 236–240.
- Lindau, J.; Dorfler, H. D.; Sackmann, H. *Z. Chem.* **1983**, *23* (2), 74–75.
- FernándezMartín, F. L.; López de la Fuente, F. L.; Cheda, J. A. R. *Thermochim. Acta* **1984**, *73* (1–2), 109–115.
- Roux, M. V.; Turrion, C.; Fernandez-Martín, F.; López de la Fuente, F. L.; Cheda, J. A. R. *Thermochim. Acta* **1989**, *139*, 139–148.
- Cheda, J. A. R.; Redondo, M. I.; García, M. V.; López-de-la-Fuente, F. L.; Fernández-Martín, F.; Westrum, E. F. *J. Chem. Phys.* **1999**, *111* (8), 3590–3598.
- Ferloni, P.; Sanesi, M.; Franzosini, P. *Z. Naturforsch.* **1975**, *30a* (11), 1447–1457.
- Ferloni, P.; Zangen, M.; Franzosini, P. *Z. Naturforsch.* **1977**, *32a* (6), 627–631.
- Sanesi, M.; Ferloni, P.; Franzosini, P. *Z. Naturforsch.* **1977**, *32a* (10), 1173–1177.
- Franzosini, P.; Sanesi, M.; Cingolani, A.; Ferloni, P. *Z. Naturforsch.* **1980**, *35a* (1), 98–102.
- White, N. A. S.; Ellis, H. A. *J. Mol. Struct.* **2008**, *888* (1–3), 386–393.
- White, N. A. S.; Ellis, H. A. *Mol. Cryst. Liq. Cryst.* **2009**, *501*, 28–42.
- Martínez Casado, F. J.; Ramos Riesco, M.; García Pérez, M. V.; Redondo Yélamos, M. I.; López-Andrés, S.; Cheda, J. A. R. *J. Phys. Chem. B* **2009**, *113* (39), 12896–12902.
- Meisel, T.; Seybold, K.; Halmos, Z.; Roth, J.; Melykúti, C. *J. Therm. Anal.* **1976**, *10* (3), 419–431.
- Meisel, T.; Sybold, K.; Roth, J. *J. Therm. Anal.* **1977**, *12*, 361–369.
- Dorfler, H. D.; Brandt, A. *Colloid Polym. Sci.* **1992**, *270* (3), 267–281.
- Dorfler, H. D.; Brandt, A.; Kolbe, A. *Colloid Polym. Sci.* **1992**, *270* (3), 282–297.
- García, M. V.; Redondo, M. I.; López de la Fuente, F. L.; Cheda, J. A. R.; Westrum, E. F.; Fernández Martín, F. *Appl. Spectrosc.* **1994**, *48* (3), 338–344.

- (50) Cheda, J. A. R.; Fernández-García, M.; Ferloni, P.; Fernández-Martín, F. *J. Chem. Thermodyn.* **1991**, *23*, 495–502.
- (51) Mc Bain, J. W.; Stewart, A. *J. Phys. Chem.* **1933**, *37*, 675–684.
- (52) Mc Bain, J. W.; Field, M. C. *J. Phys. Chem.* **1933**, *37*, 920–924.
- (53) Pacor, P.; Spier, H. L. *J. Am. Oil Chem. Soc.* **1968**, *45*, 338–342.
- (54) Brouwer, H. W.; Spier, H. L. *Proc. 3rd Int. Conf. Thermal Anal.* **1971**, *3*, 131–144.
- (55) Lynch, M. L.; Pan, Y.; Laughlin, R. G. *J. Phys. Chem.* **1996**, *100*, 357–361.
- (56) Fernández-García, M.; Cheda, J. A. R.; Westrum, E. F.; Fernández-Martín, F. *J. Colloid Interface Sci.* **1997**, *185*, 371–381.
- (57) Mirnaya, T. A.; Dradah, V. S.; Yaremchuk, G. G. *Z. Naturforsch.* **1999**, *54a*, 685–688.
- (58) Sheldrick, G. M. *SHELXS 97*; University of Göttingen: Germany, 1997.
- (59) Sheldrick, G. M. *SHELXL 97*; University of Göttingen: Germany, 1997.
- (60) Aragon, E.; Jartet, K.; Satre, P.; Sebaoun, A. *J. Therm. Anal. Cal.* **2000**, *62* (1), 211–225.
- (61) Huang, S. H.; Wang, R. J.; Mak, T. C. W. *J. Chem. Soc., Dalton Trans.* **1991**, *5*, 1379–1381.
- (62) Rietveld, H. M. *J. Appl. Crystallogr.* **1969**, *2*, 65–71.
- (63) Roisnel, T.; Rodríguez-Carvajal, J. *Mater. Sci. Forum* **2002**, *378–381*, 118–126.
- (64) Boultif, A.; Louër, D. *J. Appl. Crystallogr.* **2004**, *37*, 724–731.
- (65) Altomare, A.; Caliandro, R.; Camalli, M.; Cuocci, C.; Giacovazzo, C.; Moliterni, A. G. G.; Rizzi, R. *J. Appl. Crystallogr.* **2004**, *37*, 1025–1028.
- (66) Altomare, A.; Camalli, M.; Cuocci, C.; da Silva, I.; Giacovazzo, C.; Moliterni, A. G. G.; Rizzi, R. *J. Appl. Crystallogr.* **2005**, *38*, 760–767.
- (67) Favre-Nicolin, V.; Cerný, R. *J. Appl. Crystallogr.* **2002**, *35*, 734–743.
- (68) (a) Rodríguez-Carvajal, J. *Physica B* **1993**, *192*, 55–69. (b) Rodríguez-Carvajal, J. *Commission on Powder Diffraction (IUCr). Newsletter* **2001**, *26*, 12–19.
- (69) Busico, V.; Ferraro, A.; Vacatello, M. *J. Phys. Chem.* **1984**, *88* (18), 4055–4058.
- (70) Dumbleton, J. H.; Lomer, T. R. *Acta Crystallogr.* **1965**, *19*, 301–307.
- (71) Lewis, E. L. V.; Lomer, T. R. *Acta Crystallogr. B* **1969**, *25*, 702–710.
- (72) Macdonald, A. L.; Murray, A.; Freer, A. A.; Henderson, K. *Acta Crystallogr. C* **1995**, *51*, 404–406.
- (73) Martínez Casado, F. J.; García Pérez, M. V.; Redondo Yélamos, M. I.; Cheda, J. A. R.; Sánchez Arenas, A.; López de Andrés, S.; García-Barriocanal, J.; Rivera, A.; León, C.; Santamaría, J. *J. Phys. Chem. C* **2007**, *111* (18), 6826–6831.
- (74) Martínez Casado, F. J.; Ramos Riesco, M.; Sánchez Arenas, A.; García Pérez, M. V.; Redondo, M. I.; López-Andrés, S.; Garrido, L.; Cheda, J. A. R. *J. Phys. Chem. B* **2008**, *112* (51), 16601–16609.
- (75) Dupont, J.; de Souza, R. F.; Suarez, P. A. Z. *Chem. Rev.* **2002**, *102*, 3667–3692.
- (76) Shannon, R. D. *Acta Crystallogr. A* **1976**, *32*, 751–767.